Magnetic Resonance Imaging 107 (2024) 80–87

Contents lists available at ScienceDirect

Magnetic Resonance Imaging

journal homepage: www.elsevier.com/locate/mri

Review Article

High efficiency free-breathing 3D thoracic aorta vessel wall imaging using self-gating image reconstruction

Caiyun Shi [a,*], Dong Liang [b,c], Haifeng Wang [b], Yanjie Zhu [b,**]

[a] School of Biomedical Engineering, The Fourth Affiliated Hospital, Guangzhou Medical University, Guangzhou, China
[b] Paul C. Lauterbur Research Centre for Biomedical Imaging, Shenzhen Institutes of Advanced Technology, Chinese Academy of Science, Shenzhen, Guangdong, China
[c] Medical AI Research Centre, Shenzhen Institutes of Advanced Technology, Chinese Academy of Science, Shenzhen, Guangdong, China

ARTICLE INFO

Keywords:
Magnetic resonance imaging (MRI)
Self-gating
Thoracic aorta
Respiratory motion
Motion correction

ABSTRACT

Purpose: To improve the scan efficiency of thoracic aorta vessel wall imaging using a self-gating (SG)-based motion correction scheme.

Materials and methods: A slab-selective variable-flip-angle 3D turbo spin-echo (SPACE) sequence was modified to acquire SG signals and imaging data. Cartesian sampling with a tiny golden-step spiral profile ordering was used to obtain the imaging data during the systolic period, and then the image data were subsequently corrected based on the SG signals and binned to different respiratory cycles. Finally, respiratory artifacts were estimated from image-based registration of 3D undersampled respiratory bins that were reconstructed with L1 iterative self-consistent parallel imaging reconstruction (SPIRiT). This method was evaluated in 11 healthy volunteers and compared against conventional diaphragmatic navigator-gated acquisition to assess the feasibility of the proposed framework.

Results: Results showed that the proposed method achieved image quality comparable to that of conventional diaphragmatic navigator-gated acquisition with an average scan time of 4 min. The sharpness of the vessel wall and the definition of the liver boundary were in good agreement with the navigator-gated acquisition, which took approximately above 8.5 min depend on the respiratory rate. Further valuation of this technique in patients will be conducted to determine its clinical use.

1. Introduction

Thoracic aortic atherosclerotic plaque is a major cause of ischemic stroke worldwide [1]. 3D black-blood vessel wall magnetic resonance imaging has been demonstrated to be a promising technique for the assessment of thoracic aortic plaques [2]. It usually uses a variable-flip-angle 3D turbo spin-echo (SPACE) sequence with a diaphragmatic navigator to minimize respiratory motion during free breathing. This technique faces two issues. The first issue is the low scan efficiency, resulting in a long scan time since only a small fraction of the acquired data is acceptable for reconstruction. The scan time is further prolonged when the imaging subjects have highly irregular breathing patterns or drift in respiratory motion occurs during navigator-gated scanning. The second issue is the robustness of the navigator method. This technique is based on the hypothesis that the motion between the diaphragm and heart has a strong correction. Then, heart motion can be corrected using the estimated superior–inferior (SI) motion of the diaphragm multiplied by an empirical correction factor (typically 0.6). However, the actual correction factor varies among individuals [3,4], which cannot be adjusted accurately. In addition, many studies have demonstrated that respiratory motion not only occurs in the SI direction [5] but also causes othersrigid motion or vascular deformation [6,7].

To address the above issues, the “self-gating (SG)” technique has been proposed to correct respiratory motion while maintaining a high acquisition efficiency. This approach extracts the respiratory motion displacement directly from the acquired k-space lines integrated during image acquisition and then corrects the motion in the acquired data using this information [8]. It allows a much larger acceptance window than conventional diaphragmatic navigator-gated acquisition with an increased scan efficiency close to 100%. In addition, SG lines are

* Corresponding author at: School of Biomedical Engineering, The Sixth Affiliated Hospital, Guangzhou Medical University, Guangzhou 511436, China.
** Corresponding author at: Paul C. Lauterbur Research Centre for Biomedical Imaging, Shenzhen Institutes of Advanced Technology, Chinese Academy of Sciences, Shenzhen, Guangdong 518055, China.
E-mail addresses: caiyunshi@gzhmu.edu.cn (C. Shi), yj.zhu@siat.ac.cn (Y. Zhu).

https://doi.org/10.1016/j.mri.2024.01.009
Received 21 September 2023; Accepted 14 January 2024
Available online 17 January 2024

acquired in the heart region, allowing a more accurate estimation of motion displacement than diaphragmatic navigator-gated acquisition.

SG techniques can be divided into two groups. The first group employs radial trajectories, including 3D radial and stack of stars trajectories [9,10]. The k-space center points in the stack of stars or lines along the SI direction in the 3D radial direction are used as SG data. However, the radial trajectory requires precalibration due to hardware imperfections and has a very high computational complexity for reconstruction, particularly in iterative reconstruction of compressed sensing (CS) [11,12]. In the second group, the Cartesian trajectory is used in the SG technique by acquiring additional SG lines. It acquires data along spiral-like [13] or radial-like [14] interleaves on a Cartesian grid to achieve a variable-density sampling pattern, which can be used naturally for CS reconstruction. Most SG techniques use balanced steady-state free precession (bSSFP) or gradient echo (GRE) sequences, having bright blood signals and sufficient signal-to-noise ratios (SNRs) to extract motion displacement accurately. However, thoracic vessel wall imaging is a black-blood technique acquired with SPACE and may have a low SNR in the SG data relative to bSSFP or GRE sequences.

In this study, we propose a novel SG approach for thoracic vessel wall imaging with 100% scan efficiency. Imaging is performed using a modified SPACE sequence with the first two echoes collecting the SG data. The Cartesian k-space data are acquired using spiral profile ordering with a tiny golden-angle approach. The acquired data are binned into multiple respiratory states based on the motion displacements from the SG data. The images are reconstructed using L1 iterative self-consistent parallel imaging reconstruction (SPIRiT) [15] for each bin and are combined into one image after rigid image registration. Note that the use of a tiny golden angle is helpful to ensure that each bin has a reasonable calibration line number. The feasibility of the proposed method was demonstrated in 11 healthy subjects in about a 4 min free-breathing acquisition. The results were compared against conventional diaphragmatic navigator-gated acquisition with an average scan time of 8.5 min to assess the superiority of the proposed framework.

2. Methods

The proposed approach has four steps. In the first step, image acquisition (including the SG and imaging data) is performed using a modified SPACE sequence with a tiny golden-angle step Cartesian trajectory. Second, the amount of respiratory motion estimated from the SG data is used to correct the acquired data, which are then divided into multiple bins according to their amounts of respiratory motion. Third, the 4D volumes (3D + respiratory bins) are reconstructed for each bin, and image-based registration is performed to estimate the tissue deformation between the binned images. Finally, the registered binned images are averaged to obtain the final image. The following sections describe all the steps in further detail, as well as the experiments performed to validate this approach.

2.1. The modified SPACE sequence and data acquisition

The modified SPACE sequence is shown in Fig. 1(a). The first two echoes, which are usually discarded in conventional SPACE sequences, are acquired using two additional readouts (SG1 and SG2) in the SI direction, without any gradient encoding. The Fourier transforms of these

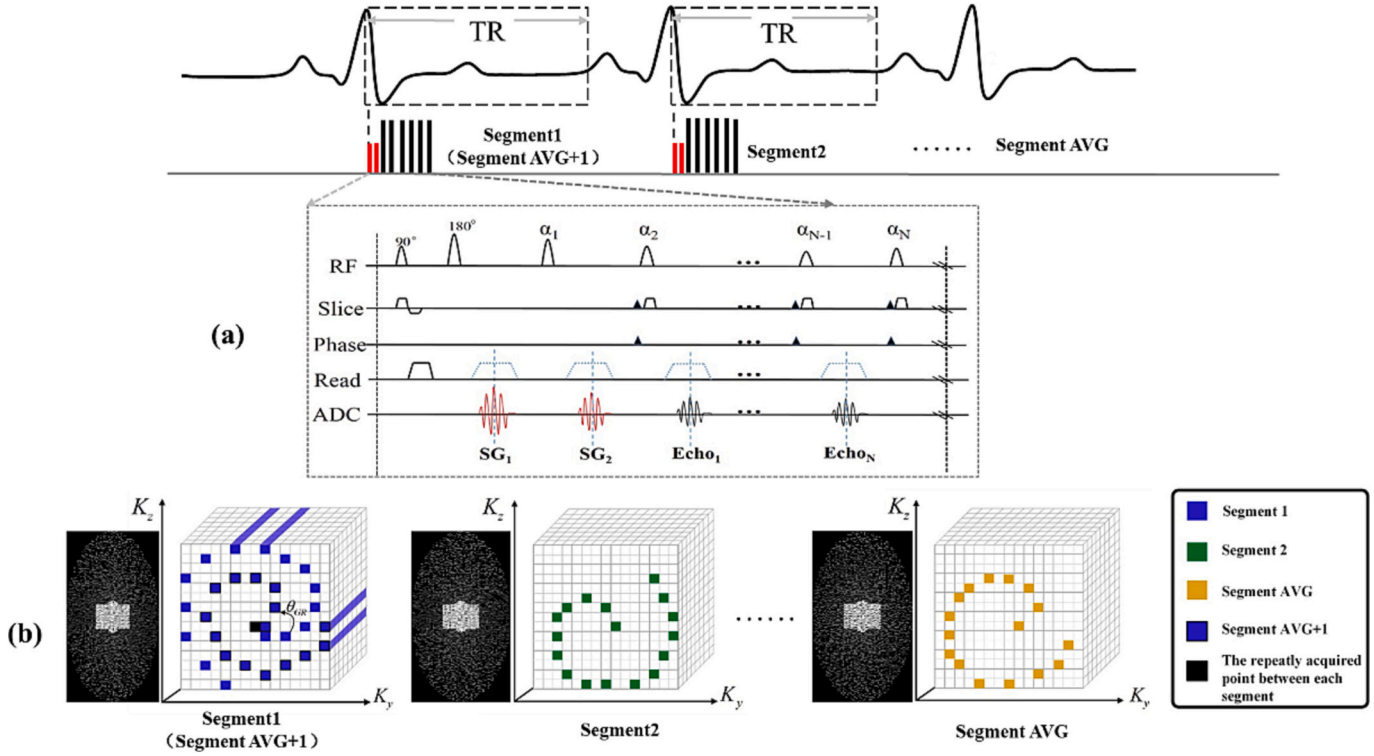

Fig. 1. The sequence diagram of the PD-weighted SG-SPACE sequence and corresponding k-space sampling pattern. a: The first two readouts in the SI direction, which were collected as SG data. The remaining echoes were collected as the thoracic aorta imaging data at each segment (~40 echoes/segment). All of the readouts were obtained in the systolic period. b: Simplified illustration of the k-space sampling strategy. After each red arrow, which was seen as the SG data, the 3D thoracic aorta imaging data were acquired using a golden-step Cartesian spiral profile ordering sampling trajectory (one spiral interleaf per heartbeat), where the angular step between two spiral interleaves in the same profile ordering was given by a tiny golden angle (θ_{GR}) = 23.6°. Each spiral interleaf (each segment) was consecutively placed on three different 3D variable-density k-space undersampling masks. Each mask had a fully sampled k-space center area with a size of 32 × 22 for calibration in the L1-SPIRiT reconstruction. Each 3D acquisition was undersampled by a factor of 2.5 with 3 repetitions (if repetition/Average = AVG = 3). Some autocalibration lines of the calibration region in each undersampling mask were repeatedly sampled. (For interpretation of the references to colour in this figure legend, the reader is referred to the web version of this article.)

lines are the 1D projections of the entire image volume, i.e., the SG lines, and are used for detecting respiratory motion. Next, the undersampled 3D thoracic aorta imaging data (accelerated factor = 2.6) are collected during the systolic period using a variable-density Cartesian trajectory with spiral profile order in the ky-kz plane (one spiral interleaf per heartbeat) [13]. The angular step between two spiral interleaves in the same profile ordering is given by a tiny golden angle of $\theta_{GR} = 23.6$ (Fig. 2(b)) [16,17]. Using the tiny golden angle can diminish transient effects such as eddy currents originating from the golden step between two interleaves. Repetitions of the sequence are 3 with different k-space undersampling masks similar to the reference are performed [18]. Each mask has a fully sampled k-space center area with a size of 32 × 22 for calibration in the L1-SPIRiT reconstruction (see Fig. 1(b)). The calibration region in each undersampling mask was oversampled [14,17], which could ensure sufficient samples in the autocalibration lines for each respiratory bin in the later respiratory step.

2.2. Motion estimation and correction

SI translation motion of the thoracic aorta is detected using the across correlation method by averaging the 1D Fourier transform of the two acquired SG lines. The reference SG line is manually selected from the end-expiration. The cross-correlation between the reference and every SG line is then calculated as follows:

$$C(u) = \frac{\sum_x [(f_u - \overline{f_u})(r - \overline{r})]}{\sigma_f(u)\sigma_r} \quad (1)$$

Where f is the SG profile, r is the reference template, and u is the translation. f_u and $\sigma_f(u)$ are the average value and standard deviation of the profile within the template window, respectively, and $\overline{r}$ and σ_r are the corresponding average and standard deviation for the reference template, respectively. The respiratory position d is then defined as the translation value (in pixels), which is the largest normalized cross-correlation [19]:

$$d = argmax_{u \in R} C(u) \quad (2)$$

Examples of SG profiles and the corresponding detected SI translation motion d are shown in Fig. 2. The SI translation motion detected is used for correcting the respiratory motion in the SI direction directly from k-space data using the Fourier shift theorem [20]. The Fourier shift theorem modulates the k-space data with a linear phase to correct the SI motion of the thoracic aorta, which in the image domain corresponds to a translational shift. 1D translational correction in the SI direction is applied within each bin separately by the corresponding phase shift in k-space prior to reconstruction:

$$\mathrm{K} = \mathrm{K}' e^{-2\pi i x \bullet d} \quad (3)$$

Where K is the translation-corrected k-space, K′ is the acquired k-space, x is the k-space index along the encoding direction x, and d is the estimated 1D translation vector.

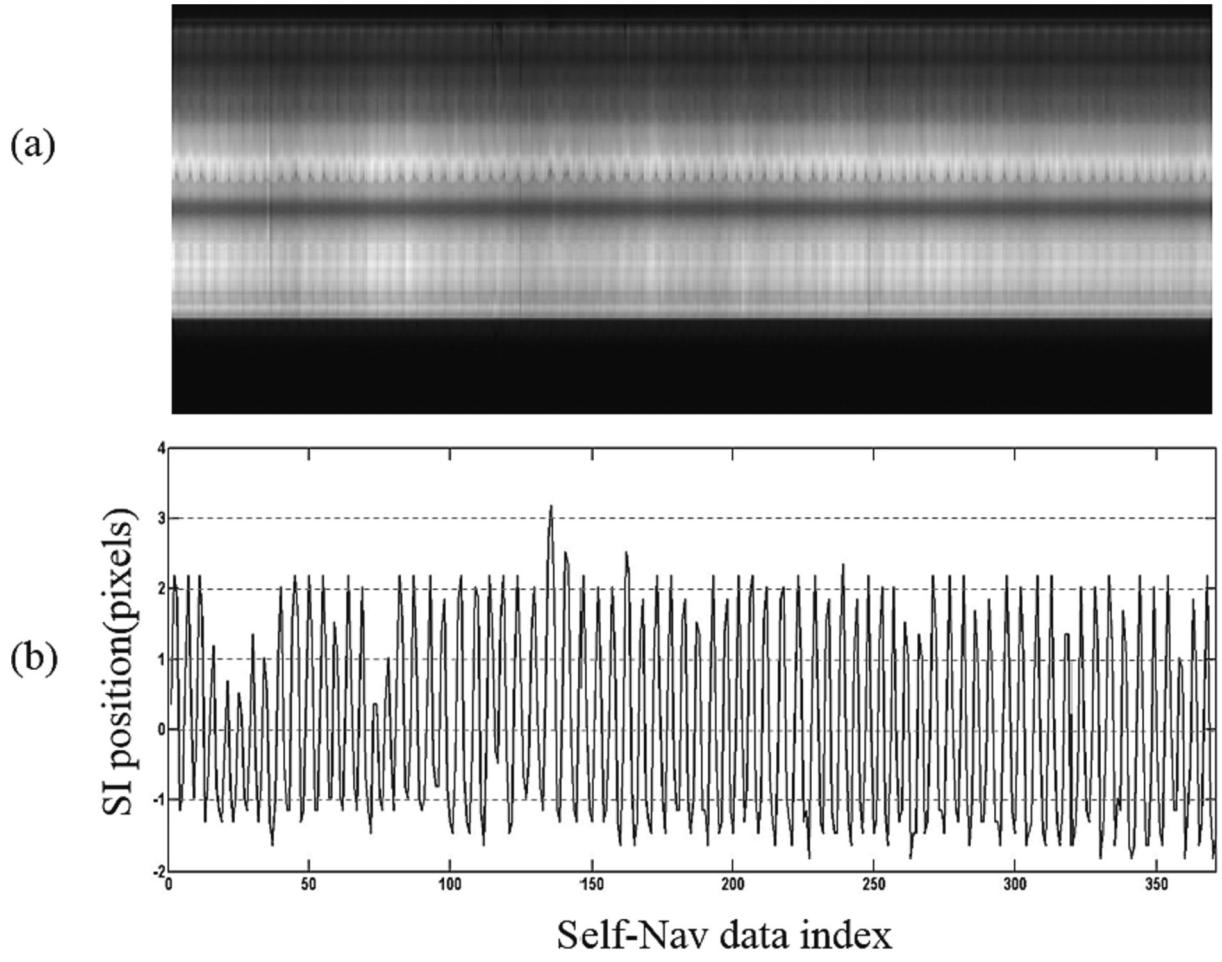

Fig. 2. (a) Time series of the self-navigation profiles. (b) Detected SI motion of the thoracic aortic. The translationally corrected data were distributed into N_{bins} respiratory bins (dashed horizontal lines). Each bin was chosen to be "soft" (i.e., adjacent breathing states overlapped by a certain amount of 15% depending on the data in each bin [not shown in the Figure]).

2.3. Image reconstruction and bin-to-bin rigid motion estimation

After translational correction, the corrected k-space data are divided into N_{bins} respiratory bins (dashed horizontal lines in Fig. 2(b)) according to their positions in the breathing cycle. Each bin is chosen to be "soft", i.e., adjacent breathing states overlap by a certain amount of 15% depending on the data of each bin (not shown in Fig. 2(b)). This approach ensures that all k-space bins contain a sufficient amount of data for stable CS imaging reconstruction. The acceleration factor of the 3D bins that are greater than eight can be rejected for reconstruction. Then, we use the L1-regularized SPIRiT approach to reconstruct the data of each bin. The reconstruction can be written as an unconstrained optimization problem:

$$\widehat{B}_n = \underset{I_n}{argmin}||DB_n - K_n||_2^2 + \lambda_1||(G-I)B_n||_2^2 + \lambda_2||\Psi\{IFFT(B_n)\}||_1 \quad (4)$$

$$n = 1 \cdots N_{bins}$$

Where operator D selects only acquired k-space locations, B_n are the reconstructed k-space data of each bin, and K_n is the data acquired at each respiratory bin after 1D translational motion correction [21,22]. G is an interpolation operator that convolves the entire k-space of each bin with the SPIRiT kernel. $\Psi\{\}$ is a wavelet operator. We solve Eq. (4) using the projection onto convex sets (POCS) algorithm [15]. Once each individual respiratory bin image $\widehat{B}_n$ is reconstructed, the bin with the lowest undersampling factor is used as a reference to estimate bin-to-bin 3D rigid deformation fields via image registration as described in reference [21]. Affine transformations are used to correct the rigid respiratory motion of the thoracic aorta. Finally, the registered bin images are averaged and combined to obtain the final image. The motion correction and reconstruction scheme are shown in Fig. 3.

2.4. Experiments

Eleven healthy volunteers (average age 32 ± 7.6 years old, 2 females and 9 males) were recruited for the study. All the thoracic aorta MRI examinations were performed on a 3 T MRI scanner during free breathing (u790, United imaging, Shanghai, China). This study was approved by our institutional review board, and written informed consent was obtained before each experiment. A 12-channel phased array abdomen coil and an integrated spine matrix coil (total of 24 channels) were used for data acquisition. MR images of the whole thoracic aorta using an oblique sagittal orientation were acquired using a conventional diaphragmatic navigator-gated acquisition and the proposed method. The imaging parameters were as follows: echo time (TE)/repetition time (TR) = 7.84/800–1000 ms, echo train length of 40, field of view (FOV) of 292 × 292 × 78 mm^3, matrix size of 224 × 224 × 60, average = 3, spatial resolution = 1.3 mm isotropic, trigger delay = 0 ms, bandwidth = 740 Hz/pixel, and spectral presaturation with inversion recovery (SPIR) preparation pulse was used for fat suppression. The conventional diaphragmatic navigator-gated acquisition was performed as a reference, which was acquired using a conventional variable-density Cartesian sampling (accelerated factor = 2) [23] and was reconstructed by the CS-based method available by the vendor. The imaging parameters were the same as above for the SG method. The acceptance window was 1 mm. Notably, the average scan time with the proposed motion correction technique was 4.0 ± 0.5 min with a 100% scan efficiency. The average scan time for the diaphragmatic navigator-gated acquisition method was 8.5 ± 1.5 min with a 20–30% scan efficiency. Therefore, the proposed acquisition method was approximately 2.1 times faster than the diaphragmatic navigator-gated acquisition method.

The images obtained by the proposed SG technique were reconstructed both with the proposed motion correction method and without motion correction. They were reconstructed for each volunteer with the L1-SPIRiT reconstruction method. After the 1D motion -corrected k-space data, these data were segmented into three to six respiratory bins according to their positions in the breathing cycle. The acceleration factor for each bin was in the range from 2.4 to 8 depending on the respiratory position and breathing pattern. The image of the bin with the lowest undersampling factor (usually end-expiration) was considered as a reference, and the images at the remaining respiratory positions were registered to that bin.

All reconstructions were implemented in MATLAB (R2014b, The MathWorks, Inc., Natick, MA, USA) on a workstation with two 10-core 2.60-GHz Intel Xeon processors (Intel Xeon E5-2660V3 and 128 GB memory). The value of the wavelet regularization parameter λ was determined empirically by comparing the reconstructions with different λs based on the balance between the blurring artifacts and noise-like artifacts in the reconstructions. The optimal value of λ was 0.01.

In addition, the study was conducted in consistent with the Declaration of Helsinki (as revised in 2013). It was approved by the Ethics Committee at the Shenzhen Institute of Advanced Technology, Chinese Academy of Sciences (The approval number of Ethics Committee is SIAT-IRB-180315-H0228), and the written informed consent was obtained before experiments from all patients.

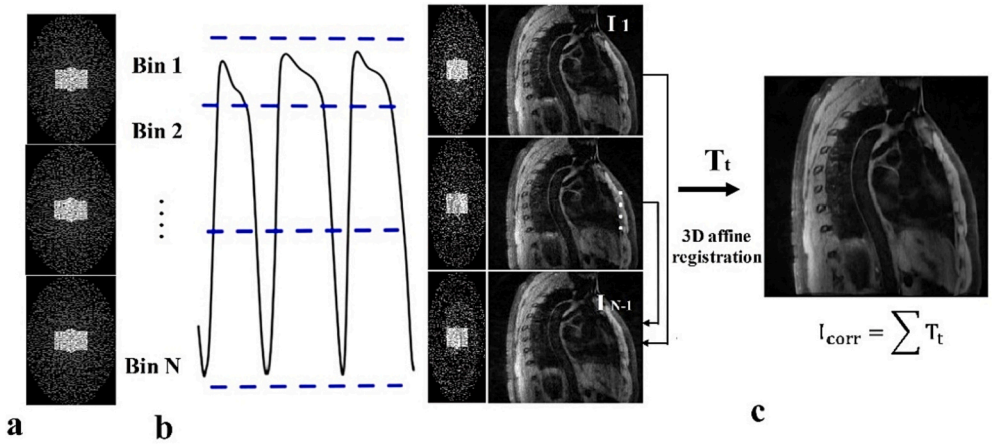

Fig. 3. Proposed approach. a: The three variable-density sampling masks of the UIH scanner. b: The acquired data were binned into different respiratory positions, and the respiratory artifacts in the SI direction were corrected according to their position in the respiratory signal given by a 1D SG echo. The undersampled data in each bin were then reconstructed using L1-SPIRiT to obtain respiratory-resolved undersampled images that could be registered to a common respiratory position. c: 3D image-based affine registration was executed, and motion-corrected thoracic MR images were obtained by combining each registered bin.

2.5. Data analysis

For each healthy subject, all the thoracic aorta images with three different orientations (transverse view, coronal view and sagittal view) were comprehensively evaluated by 2 independent readers with at least 5 years of experience in cardiovascular imaging who were blinded to the techniques employed. The reconstruction results were compared in terms of visualized thoracic aorta vessel delineation, sharpness and motion artifacts. The overall image quality was graded using a four-point scale (0–3), where 0 indicates poor quality (unidentifiable and completely blurred lumen and wall); 1 indicates fair quality (identifiable but heavily blurred lumen and wall); 2 indicates good quality (well-defined lumen and wall with slight artifacts); 3 indicates excellent quality (excellent visualization and sharp vessel wall and lumen margins with no artifacts). The final image-quality score was determined as an average of the scores across the 2 readers. The quantitative differences between the diaphragmatic navigator-gated acquisition results and the results of the proposed SG method were tested for statistical significance using a paired *t*-test ($P < 0.05$).

3. Results

Representative results of the thoracic MR images with three different views are shown in Fig. 4. The reconstructed volumes of the thoracic aorta by the proposed method (Corrected) showed a vessel definition and sharpness comparable to the diaphragmatic navigator-gated acquisition results (Reference) since the proposed method reduces the motion artifacts by suppressing respiratory motion during image reconstruction. Motion artifacts can be seen in the noncorrected acquisition images on both the coronal and transverse views (the red arrow in Fig. 4 on the coronal and transverse views). Without any motion correction, the vessel was blurry and the thoracic aorta was poorly visualized under the same acquisition time as the proposed technique.

In several volunteers with shallow respiration (3 out of the 11 volunteers), the vessel wall of the thoracic aorta was clearly depicted in some views, such as the sagittal view for all three methods (Fig. 5). However, the proposed approach still showed improved image quality and reduced artifacts compared with the noncorrected approach (see the coronal and transverse views). Therefore, the proposed approach could provide better-quality images of the thoracic aorta under any breathing pattern conditions.

The analysis of the quality measurements for all 11 volunteers is shown in Fig. 6. The means and standard deviations of the image-quality scores were 2.26 ± 0.50, 2.33 ± 0.47, and 1.49 ± 0.26 for the navigator-gated, corrected and noncorrected acquisitions, respectively. The score of the proposed method was comparable to that of the Navigator-gated approach ($P = 0.87$) and significantly higher than that of the non-corrected approach ($P < 0.05$).

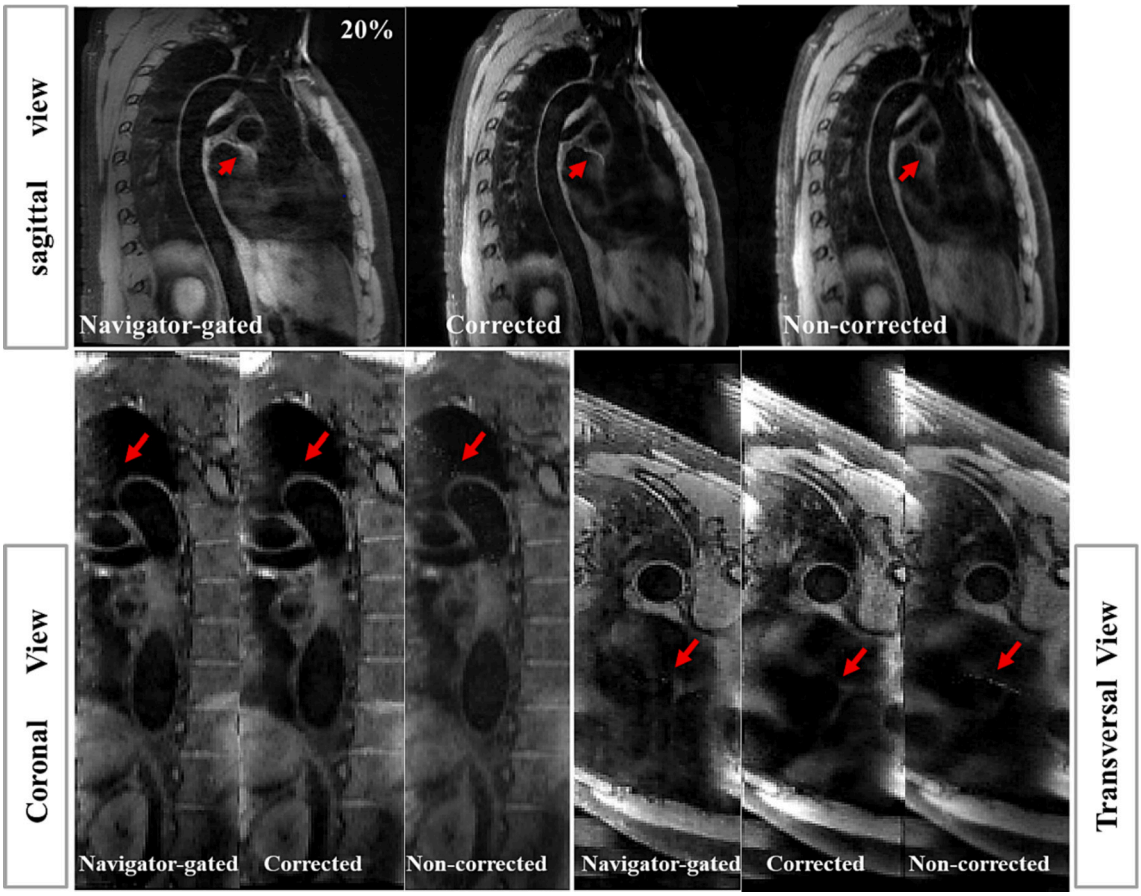

Fig. 4. Representative results of the thoracic MRI scans with three different views under the united imaging scanner. Navigator-gated: navigator-gated acquisition with an image acquisition rate of 20% (acquisition time: 9 min). Corrected: ungated acquisition reconstructed with the proposed motion correction approach. Noncorrected: ungated acquisition with no motion correction (acquisition time: 4 min). A good depiction of the aortic arch was observed with both the navigator-gated and corrected approaches. Blurring could be observed in the vessel wall when no motion correction was performed (arrow shown on the sagittal view). Motion artifacts can be seen in the noncorrected acquisition on both the coronal and transverse views (See the red arrows). Scan efficiency was indicated on the superior right-hand side of the navigator-gated image. (For interpretation of the references to colour in this figure legend, the reader is referred to the web version of this article.)

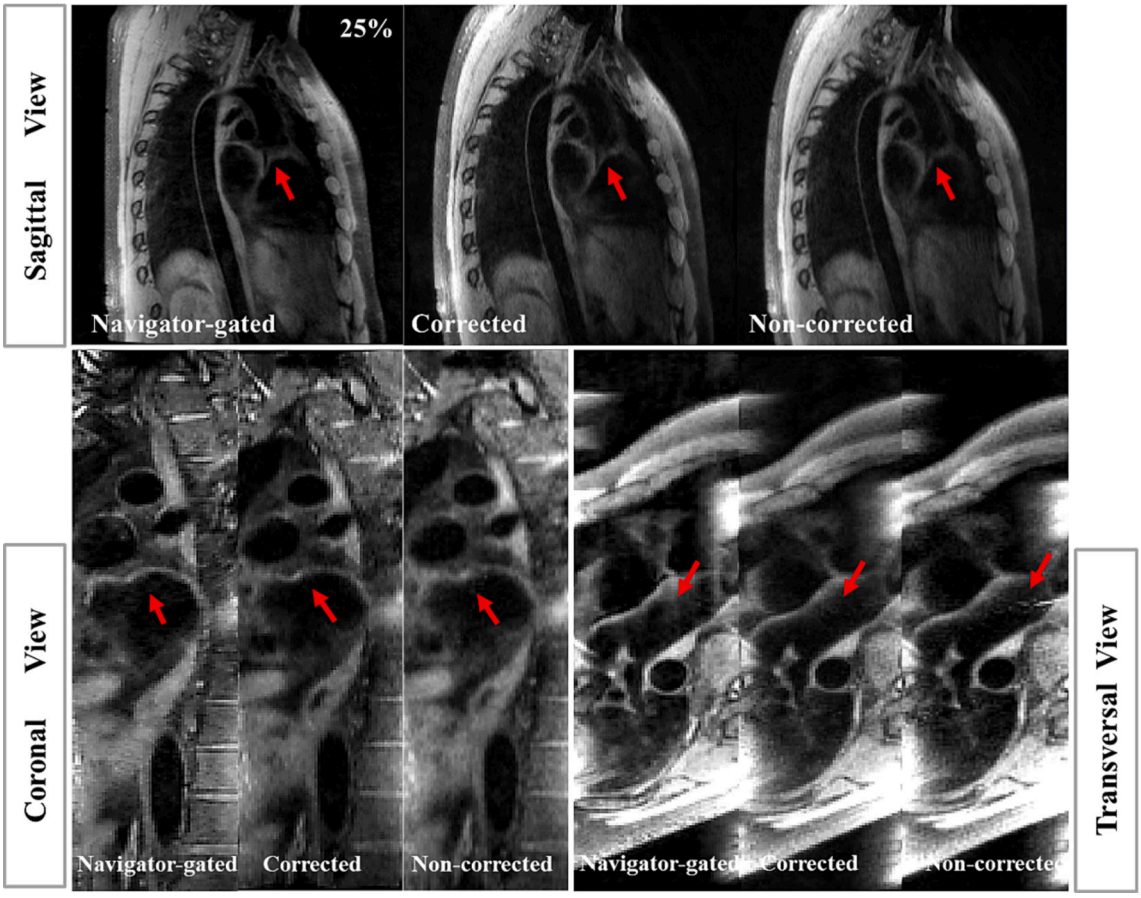

Fig. 5. The results of the thoracic MRI scans from one volunteer. Navigator-gated: navigator-gated with an image acquisition rate of 25% (acquisition time: 8.5 min). Corrected: ungated acquisition reconstructed with the proposed motion correction approach. Noncorrected: ungated acquisition with no motion correction (acquisition time: 4 min). Obvious respiratory movement artifacts are appeared in coronal and transversal views of the noncorrected images(See the red arrow). (For interpretation of the references to colour in this figure legend, the reader is referred to the web version of this article.)

4. Discussion

One of the major challenges to overcome in cardiac imaging of the aorta is performing imaging in the presence of physiological movement, i.e., cardiac pulsation and respiration. Conventional cardiovascular MRI techniques adopt electrocardiography (ECG) in a quiescent cardiac phase (usually mid-diastole) and breath-holding for data acquisition or diaphragmatic navigator-gated acquisition with a low-rate acceptance window to resolve respiratory motion. In this work, an SG approach for 3D affine respiratory motion correction was proposed for thoracic aorta imaging. Respiratory self-navigation is obtained from a k-space readout along the SI direction before acquiring the imaging data. 1D translational intra-bin respiratory drifts are corrected according to the SG data, and the inter-bin rigid motion artifacts can be corrected by using the respiratory bin's strategy and 3D affine image registration. The results show that the proposed method can achieve 3D thoracic aorta vessel wall imaging under free-breathing conditions within ~4 min and yield comparable thoracic aorta vessel visualization compared with the diaphragmatic navigator-gated approach. On average, the proposed method reduces the acquisition time by 2.1 min compared with the diaphragmatic navigator-gated approach.

The spiral-order Cartesian trajectory has been widely used in previous SG MRI applications. In our study, two strategies were employed to improve the overall performance of the method. The first is oversampling the calibration region in the k-space center during acquisition to guarantee that each respiratory bin has sufficient calibration lines in the respiratory bin step. The second is using a tiny golden angle instead of the traditional golden angle, which can reduce eddy current artifacts originating from k-space jumps between consecutive spiral interleaves. To show the eddy current effects from the trajectory, transverse views of the thoracic aorta for different golden angles are shown in Fig. 7. The aortic vessel wall becomes invisible as the golden angle increases. When using a tiny golden angle of 23.6°, well-defined lumen and vessel definitions are obtained (red arrow). In our future work, we will investigate the sampling pattern of radial-like Cartesian trajectory [24], which may be particularly suitable for the respiratory binning step.

In the respiratory bin's strategy, residual rigid motion can be further reduced by increasing the number of bins. However, the undersampling factor of each bin will increase, which may reduce the quality of the reconstructed images. Therefore, three to six respiratory bins with accelerated factors of 2.4–8.0 were employed in our study since this resulted in a reasonable tradeoff between the bin size and the amount of data within each bin. To minimize intra-bin motion for each bin, 1D translational motion correction is performed before reconstructing each bin's images. Good results are achieved with this strategy for highly efficient thoracic aorta imaging.

Our study has some limitations. First, all the imaging data were obtained in the systolic period to realize black-blood imaging. However, in patients with cardiac arrhythmias, this strategy may result in severe motion artifacts. Second, high-SNR images are highly desirable to better delineate the vessel wall. To improve the SNR, multiple repetitions are often used in conventional acquisition, but this method prolongs the scan time. In the future, additional reconstruction models, such as patch-based low-rank approximation [25], can be used for image reconstruction and may achieve better performance in improving the image SNR while using single-repetition imaging data. Third, the proposed method

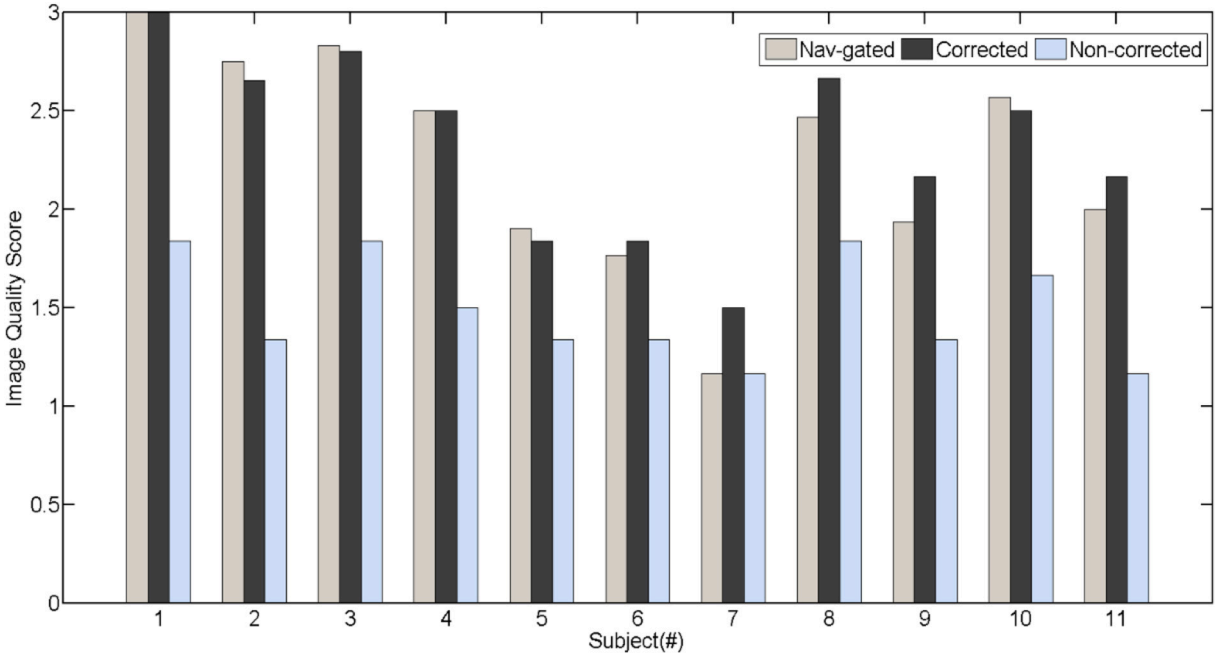

Fig. 6. Qualitative (visual score) analysis results from healthy volunteers with scoring criteria of 0–3. The average values of the overall image-quality scores are given by two readers over all 11 subjects for each imaging method. For the proposed motion correction technique (corrected), the average image-quality scores were >1.5. However, the average image-quality scores of the noncorrected acquisitions were <1.5 for most of the volunteers, which was not enough for clinicians and radiologists to obtain clinically related information. *Statistically significant differences ($P < 0.05$).

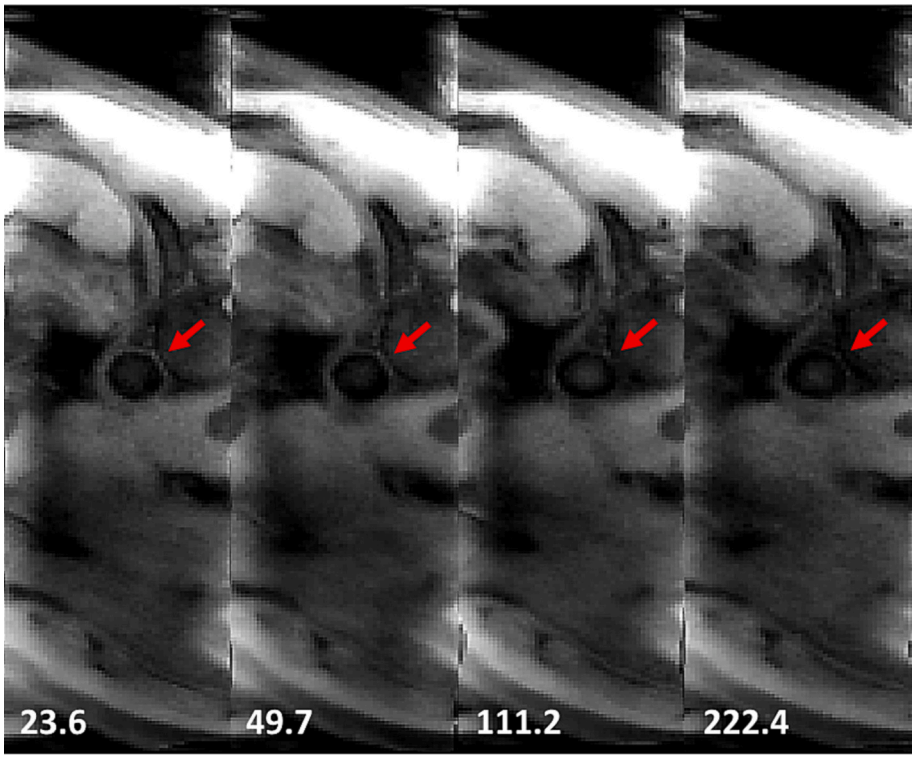

Fig. 7. The transversal views of the thoracic aorta with different golden angles. The aortic vessel wall becomes invisible as the golden angle increases. A well-defined lumen and better vessel definition is obtained if a tiny golden angle of 23.6° is used (red arrow). (For interpretation of the references to colour in this figure legend, the reader is referred to the web version of this article.)

requires a 2.6-h reconstruction time with nonoptimized MATLAB code. Although the computational efficiency of this method is much higher than the radial approach proposed by Bhat et al. and Pang et al. [19,26], which uses a 16-h reconstruction time, the reconstruction time is still too long for clinical use. In our future work, channel compression techniques [27,28], graphics processing unit (GPU)-based implementation [29,30] and other techniques will be used to reduce the reconstruction time to a clinically acceptable range of 1–5 min. Finally, the preliminary

feasibility and reliability of the proposed method is tested only on healthy volunteers. Patients need to be recruited to test the sensitivity and specificity of this technique with respect to different types of thoracic aortic diseases. We will validate the proposed technique on a large patient cohort in our future work.

5. Conclusions

In conclusion, we proposed an SG thoracic aorta vessel wall imaging method with 100% scan efficiency and an affine respiratory motion correction technique. This technique estimates respiratory motion from the SG data and corrects this motion during the reconstruction process. The results demonstrate that the proposed method yields image quality comparable to that of 1-mm navigator-gated acquisition with a longer scan time and outperforms noncorrected acquisition with the same acquisition time. Further evaluation of the proposed method in healthy volunteers and patients will be conducted in the future.

Declaration of competing interest

None.

Acknowledgments

This work was partially supported by grants from the National Key R&D Program of China (2021YFF0501402), Guangzhou Medical University Research Capability Enhancement Project (02-410-2405125) the National Natural Science Foundation of China (62322119, 81901736, 12226008, 61871373, 81830056, 62201561 and 81971611), the Strategic Priority Research Program of the Chinese Academy of Sciences (XDB25000000 and XDC07040000), Guangdong Basic and Applied Basic Research Foundation (2021A1515110540), the Engineering Laboratory Program of the Chinese Academy of Sciences (KFJ-PTXM-012), the High-level Talent Program in the Pearl River Talent Plan of Guangdong Province (2019QN01Y986), the Shenzhen Science and Technology Program (RCYX20210609104444089 , JCYJ20220818101205012, JCYJ20210324115810030), the Science and Technology Plan Program of Guangzhou (202007030002). The Key Technology and Equipment R&D Program of Major Science and Technology Infrastructure of Shenzhen (202100102 and 202100104).

References

[1] Amarenco P, Cohen A, Tzourio C, Bertrand B, Hommel M, Besson G, et al. Atherosclerotic disease of the aortic arch and the risk of ischemic stroke. N Engl J Med 1994;331:1474–9.
[2] Zhang Z, Fan Z, Carroll TJ, Chung YC, Weale P, Jerecic R, et al. Three-dimensional T2-weighted MRI of the human femoral arterial vessel wall at 3.0 tesla. Invest Radiol 2009;44:619–26.
[3] Taylor AM, Keegan J, Jhooti P, Firmin DN, Pennell DJ. Calculation of a subject-specific adaptive motion-correction factor for improved real-time navigator echo-gated magnetic resonance coronary angiography. J Cardiovasc Magn Reson 1999;1:131–8.
[4] Danias PG, Stuber M, Botnar RM, Kissinger KV, Edelman RR, Manning WJ. Relationship between motion of coronary arteries and diaphragm during free breathing: Lessons from real-time MR imaging. In: Am. J. Roentgenol. vol. 172. American Roentgen Ray Society; 1999. p. 1061–5.
[5] Wang Y, Riederer SJ, Ehman RL. Respiratory motion of the heart: kinematics and the implications for the spatial resolution in coronary imaging. Magn Reson Med 1995;33:713–9.
[6] Manke D, Nehrke K, Börnert P, Rösch P, Dössel O. Respiratory motion in coronary magnetic resonance angiography: a comparison of different motion models. J Magn Reson Imaging 2002;15:661–71.
[7] Shechter G, Ozturk C, Resar JR, McVeigh ER. Respiratory motion of the heart from free breathing coronary angiograms. IEEE Trans Med Imaging 2004;23:1046–56.
[8] Pang J, Sharif B, Fan Z, Bi X, Arsanjani R, Berman DS, et al. ECG and navigator-free four-dimensional whole-heart coronary MRA for simultaneous visualization of cardiac anatomy and function. Magn Reson Med 2014;72:1208–17.
[9] Spincemaille P, Liu J, Nguyen T, Prince MR, Wang Y. Z intensity-weighted position self-respiratory gating method for free-breathing 3D cardiac CINE imaging. Magn Reson Imaging 2011;29:861–8.
[10] Liu J, Spincemaille P, Codella NCF, Nguyen TD, Prince MR, Wang Y. Respiratory and cardiac self-gated free-breathing cardiac CINE imaging with multiecho 3D hybrid radial SSFP acquisition. Magn Reson Med 2010;63:1230–7.
[11] Feng L, Grimm R, Obia Block KT, Chandarana H, Kim S, Xu J, et al. Golden-angle radial sparse parallel MRI: combination of compressed sensing, parallel imaging, and golden-angle radial sampling for fast and flexible dynamic volumetric MRI. Magn Reson Med 2014;72:707–17.
[12] Otazo R, Kim D, Axel L, Sodickson DK. Combination of compressed sensing and parallel imaging for highly accelerated first-pass cardiac perfusion MRI. Magn Reson Med 2010;64:767–76.
[13] Prieto C, Doneva M, Usman M, Henningsson M, Greil G, Schaeffter T, et al. Highly efficient respiratory motion compensated free-breathing coronary MRA using golden-step Cartesian acquisition. J Magn Reson Imaging 2015;41:738–46.
[14] Cheng JY, Zhang T, Ruangwattanapaisarn N, Alley MT, Uecker M, Pauly JM, et al. Free-breathing pediatric MRI with nonrigid motion correction and acceleration. J Magn Reson Imaging 2015;42:407–20.
[15] Lustig M, Pauly JM. SPIRiT: iterative self-consistent parallel imaging reconstruction from arbitrary k-space. Magn Reson Med 2010;64:457–71.
[16] Wundrak S, Paul J, Ulrici J, Hell E, Geibel MA, Bernhardt P, et al. Golden ratio sparse MRI using tiny golden angles. Magn Reson Med 2016;75:2372–8.
[17] Wundrak S, Paul J, Ulrici J, Hell E, Rasche V. A small surrogate for the golden angle in time-resolved radial MRI based on generalized fibonacci sequences. IEEE Trans Med Imaging 2015;34:1262–9.
[18] Munoz C, Neji R, Cruz G, Mallia A, Jeljeli S, Reader AJ, et al. Motion-corrected simultaneous cardiac positron emission tomography and coronary MR angiography with high acquisition efficiency. Magn Reson Med 2018;79:339–50.
[19] Pang J, Bhat H, Sharif B, Fan Z, Thomson LEJ, Labounty T, et al. Whole-heart coronary MRA with 100% respiratory gating efficiency: self-navigated three-dimensional retrospective image-based motion correction (TRIM). Magn Reson Med 2014;71:67–74.
[20] Shankaranarayanan A, Wendt M, Lewin JS, Duerk JL. Two-step navigatorless correction algorithm for radial k-space MRI acquisitions. Magn Reson Med 2001;45:277–88.
[21] Cruz G, Atkinson D, Henningsson M, Botnar RM, Prieto C. Highly efficient nonrigid motion-corrected 3D whole-heart coronary vessel wall imaging. Magn Reson Med 2017;77:1894–908.
[22] Zhang T, Cheng JY, Potnick AG, Barth RA, Alley MT, Uecker M, et al. Fast pediatric 3D free-breathing abdominal dynamic contrast enhanced MRI with high spatiotemporal resolution. J Magn Reson Imaging 2015;41:460–73.
[23] Shi C, Liu C, Su S, Wang H, Liu X, Zheng H, et al. High efficiency free-breathing 3D thoracic aorta imaging with self-navigated image reconstruction. Int Soc Magn Reson Med 2019:3884.
[24] Correia T, Cruz G, Schneider T, Botnar RM, Prieto C. Technical note: accelerated nonrigid motion-compensated isotropic 3D coronary MR angiography. Med Phys 2018;45:214–22.
[25] Hao R, Su Z. A patch-based low-rank tensor approximation model for multiframe image denoising. J Comput Appl Math 2018;329:125–33.
[26] Bhat H, Ge L, Nielles-Vallespin S, Zuehlsdorff S, Li D. 3D radial sampling and 3D affine transform-based respiratory motion correction technique for free-breathing whole-heart coronary MRA with 100% imaging efficiency. Magn Reson Med 2011;65:1269–77.
[27] Huang F, Vijayakumar S, Li Y, Hertel S, Duensing GR. A software channel compression technique for faster reconstruction with many channels. Magn Reson Imaging 2008;26:133–41.
[28] Zhang T, Pauly JM, Vasanawala SS, Lustig M. Coil compression for accelerated imaging with Cartesian sampling. Magn Reson Med 2013;69:571–82.
[29] Stone SS, Haldar JP, Tsao SC, Hwu WW, Sutton BP, Liang Z. Accelerating advanced MRI reconstructions on GPUs. J Parallel Distrib Comput 2008;68:1307–18.
[30] Smith DS, Gore JC, Yankeelov TE, Welch EB. Real-time compressive sensing MRI reconstruction using GPU computing and split Bregman methods. Int J Biomed Imaging 2012;2012:1–6.